RSC Advances

PAPER

View Article Online
View Journal | View Issue

Cite this: *RSC Adv.*, 2017, **7**, 32294

Patterning Bi_2Se_3 single-crystalline thin films on Si(111) substrates using strong oxidizing acids

Lei Gao,[ac] Handong Li,*[a] Wuyang Ren,[b] Gaoyun Wang,[a] Hui Li,[a] Zhihua Zhou,[a] Haining Ji,[a] Xiaobin Niu[a] and Zhiming Wang[b]

Received 11th May 2017
Accepted 19th June 2017

DOI: 10.1039/c7ra05317g

rsc.li/rsc-advances

Acidic potassium dichromate solutions ($K_2Cr_2O_7$–H_2SO_4 and $K_2Cr_2O_7$–HCl) are applied for patterning single crystalline Bi_2Se_3 thin films on Si(111) substrates. In solutions with appropriate component proportions, vertical walls and mesa-shaped structures on the etching profiles of (001) Bi_2Se_3 films can be achieved. Stoichiometric etching behavior is noted for Bi_2Se_3 in $K_2Cr_2O_7$–H_2SO_4 etchant, while incongruently dissolution of Bi_2Se_3 in $K_2Cr_2O_7$–HCl is observed which leaves a Se deficient layer on the etched film surface. The chemical reaction kinetics of Bi_2Se_3 in the two different etchants are also discussed.

1. Introduction

The layered compound Bi_2Se_3 has been used for thermoelectric (TE) energy conversion for years.[1,2] After being revealed as a topological insulator (TI), Bi_2Se_3 has become much more sought-after than ever before.[3] Featuring a large bulk band gap (~0.3 eV) and simple Dirac-cone shaped surface states, Bi_2Se_3 is advocated as the most promising TI for room temperature applications.[4,5] Some fingerprints of Bi_2Se_3 TI surface states have already been detected in electronic transport measurements, such as B–A interference effects,[6] anti-localization behaviors,[7] and unique anisotropic magneto-resistance.[8] These findings have promised novel quantum devices of Bi_2Se_3 beyond its traditional TE applications. Furthermore, high quality Bi_2Se_3 thin films can be readily grown on substrates such as Si,[9–11] GaAs,[12] and InP[13,14] at rather low temperatures (~500 K), which sensibly promotes bottom-up on-chip integration of Bi_2Se_3 devices.

However, as a key step towards device realization, patterning Bi_2Se_3 thin films is still of challenge. Physical bombardment of argon ions and reactive ion etching offer very little selectivity of the sample material over photoresist and carbonization of photoresist masks due to long term exposure to high energy ion beams may ensue. The complicated operation also hinders the popularity of dry-etch in processing weakly-bonded Bi_2Se_3. As compared to dry etching approaches, wet etching is an effective alternative due to its high etching rate, low cost and high selectivity. The etchants with different etching velocity, surface roughness, and some other characteristics can further be worked out for various purpose. Among etchants ever employed for Bi_2Se_3 and other chalcogenides, iodine and/or bromine based chemistries promise selective surface etching at limited rate.[15] For fast chemical cutting of bismuth chalcogenides, the most popular wet etchant ever used is aqueous solutions of HNO_3 and HCl mixture (diluted aqua regia).[16–21] However, these highly corrosive solutions could cause a vigorous uncontrollable reaction with Bi_2Se_3, resulting in severe edge undercutting. The diluted aqua regia etchants become even detrimental for handling thin films because they either cause pattern disappearance or trigger the delamination of weakly adhering Bi_2Se_3 films from bottom substrates.[22]

In this work, oxidizing etchants based on $K_2Cr_2O_7$–H_2SO_4 and $K_2Cr_2O_7$–HCl solutions are used for patterning Bi_2Se_3 thin film electrodes on Si, respectively. $K_2Cr_2O_7$–H_2SO_4–HCl ternary system has been verified suitable for using in etching solutions of covalent GaAs and InP wafers before.[23] It's demonstrated that the simpler $K_2Cr_2O_7$–H_2SO_4 and $K_2Cr_2O_7$–HCl binary aqueous solutions can also produce mesa-shaped structures with vertical walls of layered Bi_2Se_3 thin films in this research. Superior surface morphologies of the etched Bi_2Se_3 (001) over the unetched ones are obtained in solutions with proper acidities. However, incongruently etching behaviors on the Bi_2Se_3 surfaces are noted that a Se depletion surface layer is formed on Bi_2Se_3 etched in the $K_2Cr_2O_7$–HCl solutions.

2. Experimental section

Single crystalline Bi_2Se_3 thin films grown on (111)-oriented Si substrates by physical vapor deposition are adopted in this study. Details of thin film growth can be found in our previously published work.[11] The thickness of Bi_2Se_3 films involved in this study is ~300 nm. Photoresist etching mask is made by standard photolithography. About 1 μm thick resist (AZ5214) is

[a]*State Key Laboratory of Electronic Thin Films and Integrated Devices, School of Microelectronics and Solid-State Electronics, University of Electronic Science and Technology of China, Chengdu 610054, China. E-mail: hdli@uestc.edu.cn*
[b]*Institute of Fundamental and Frontier Sciences, University of Electronic Science and Technology of China, Chengdu 610054, China*
[c]*Microsystem and Terahertz Research Center, Chinese Academy of Engineering Physics, Chengdu 610200, China*

Table 1 H^+ concentration of $K_2Cr_2O_7$–HCl (H_2SO_4) etchants

Etch solution	Proportion	$[H^+]$ (mol L^{-1})
$K_2Cr_2O_7$–HCl	1 : 1	6
$K_2Cr_2O_7$–HCl	1 : 2	8
$K_2Cr_2O_7$–HCl	1 : 3	9
$K_2Cr_2O_7$–H_2SO_4	1 : 1	9
$K_2Cr_2O_7$–H_2SO_4	1 : 2	12
$K_2Cr_2O_7$–H_2SO_4	1 : 3	13.5

masked on each Bi_2Se_3 film surface by spin coating. After being prebaked for 65 seconds at 100 degree, the samples are exposed to ultraviolet light for 20 seconds. Submicron ultraviolet mask aligner is applied in this step. After removing the unexposed photoresist in developer solution and rinsed in deionized water, patterned samples are obtained. To enhance the adhesion of photoresist, all the samples are post baked for 5 minutes at 110 degree.

The $K_2Cr_2O_7$–HCl (H_2SO_4) etchants are prepared by intermixing 9 v/v% $K_2Cr_2O_7$ and 48 v/v% HCl (98 v/v% H_2SO_4) solutions in volume proportions of 1 : 1, 1 : 2, and 1 : 3 (thereafter denoted by 1 : n $K_2Cr_2O_7$–HCl (H_2SO_4), n = 1, 2, 3), respectively at room temperature. As in Table 1, the acquired acidities, as represent by H^+ concentration ($[H^+]$) in the solutions, are calculated to be 6 mol L^{-1}, 8 mol L^{-1}, and 9 mol L^{-1} for the 1 : 1, 1 : 2, and 1 : 3 $K_2Cr_2O_7$–HCl etchants, respectively. For the 1 : 1 to 1 : 3 $K_2Cr_2O_7$–H_2SO_4 etchants, $[H^+]$ values are 9 mol L^{-1}, 12 mol L^{-1}, and 13.5 mol L^{-1}, respectively. The Bi_2Se_3 films are etched in these aqueous acidic solutions for given time and no stirring is carried out to isolate the influence from hydromechanical effect. After etching, the samples are rinsed in acetone until the photoresist can be stripped. To investigate the dissolution of Bi_2Se_3, ascertain the character of corresponding reactions and determine limiting stages of the process, various methods are involved in the experiments. The thickness of the etched films is measured by a surface profilometer (Dektak150, Veeco). Optical microscopy (Olympus BX51), atomic force microscopy (AFM), and scanning electron microscopy (SEM) are employed to investigate the surface morphologies of the obtained patterns. Surface structural and compositional details of etched samples are further studied by Raman and electron dispersive spectroscopy (EDX), respectively. The chemical identification and binding energy study of the etched Bi_2Se_3 films are conducted by X-Ray Photoelectron Spectroscopy (XPS, Omicron).

3. Results and discussion

Fig. 1(a) shows a photograph of a Bi_2Se_3 film etched by using 1 : 2 $K_2Cr_2O_7$–HCl solution. A grid pattern of Bi_2Se_3 with designed 8 μm line width and 50 × 50 μm^2 windows is left on the Si substrate after thoroughly etching. Fig. 1(b) exhibits Raman curves taken from the Bi_2Se_3 grid and the etched window area of the sample, respectively. Three strong peaks locating at 71 cm^{-1}, 131 cm^{-1} and 173 cm^{-1} are attributed to the A^1_{1g}, E^2_g, and A^2_{1g} transitions of pure Bi_2Se_3 respectively,[24,25]

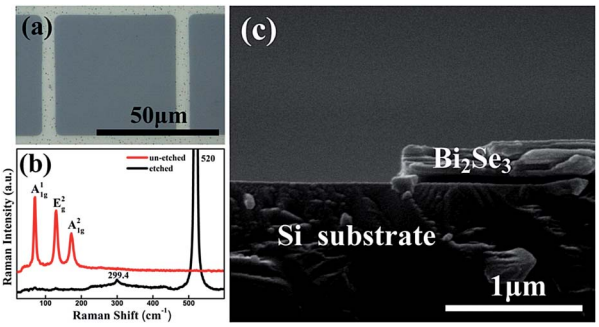

Fig. 1 (a) An optical photograph of a 1 : 2 $K_2Cr_2O_7$–HCl solution etched Bi_2Se_3 film with rectangular grid pattern. (b) Raman curves taken from the grid line (red) and window region (black) on (a), respectively. (c) Cross-sectional SEM image indicates the side-wall structure of the etched Bi_2Se_3 film in (a).

which indicates a good crystallinity of the un-etched part of Bi_2Se_3 film. While there are only two peaks of Si(111) (299.4 cm^{-1} and 520 cm^{-1}) found on the Raman spectrum from the etched area, indicating a complete removal of Bi_2Se_3 without any deposits left on the Si substrate after chemical reaction. A cross-sectional SEM image of the etched Bi_2Se_3 pattern further manifests the details at the edge of the etched Bi_2Se_3 film. As shown in Fig. 1(c), the side wall of the etched groove is straight and perpendicular to the horizontal surface of Bi_2Se_3 film which unambiguously depicts the superiority of the acid $K_2Cr_2O_7$ solution in obtaining mesa-shape microstructures of Bi_2Se_3.

For better describing the dissolving properties of Bi_2Se_3 in acid $K_2Cr_2O_7$ solutions, the etching depths (θ) of the Bi_2Se_3 film are measured at different time intervals (t). A typical θ–t curve of Bi_2Se_3 in 1 : 2 $K_2Cr_2O_7$–HCl etchant is shown in Fig. 2(a), and a constant etching rate of ~120 nm min^{-1} is calculated from its linear fitting, indicating a rate-controlled etching reaction. It must be pointed out that the etching almost ceases at depth of 350 nm which is possibly due to the consumption of $[H^+]$ in the solution. Also noted from the θ–t curve is the reaction delay of Bi_2Se_3 during the initial 15 seconds before the balanced etching rate can be reached. Such behavior is also observed in all other reactions. By carefully excluding any extrinsic contamination on sample surfaces, we suppose the initial dissolving of Bi_2Se_3 is hindered by a thick native oxidized layer formed on each sample surface which has suffered long-time exposure in air. The induction period varies a lot for different Bi_2Se_3 samples, despite of the same acidity and temperature conditions are adopted in those reactions, which is ascribed to the reaction dependence on different chemical compositions and/or thicknesses of the oxidized layers on Bi_2Se_3 samples, and would not be discussed here. After the induction period, the reaction accelerates and the dissolving process of Bi_2Se_3 exhibits clear dependence on both the reaction temperatures and acidities of the etchants. Fig. 2(b) shows the quantitative Bi_2Se_3 etching rate dependence on acidities of $K_2Cr_2O_7$–HCl and temperatures (20 °C to 45 °C). In the $[H^+]$: 6 mol L^{-1} etchant, the chemical reaction is weak that rather slight dissolution of the film can be detected even after the solution temperature is elevated from 20 °C to 45 °C (actually, the etching rate is only increased from

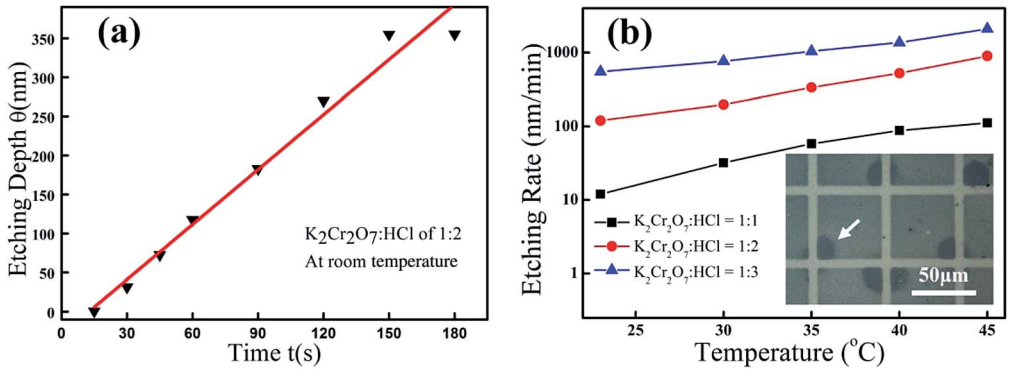

Fig. 2 (a) Time-dependent etching depth evolution of Bi_2Se_3 in 1 : 2 $K_2Cr_2O_7$–HCl solution. (b) Temperature-dependent etching rates of Bi_2Se_3 in 1 : 1, 1 : 2, and 1 : 3 $K_2Cr_2O_7$–HCl solutions, respectively. Inset in (b) is a typical optical microscopic picture taken from a Bi_2Se_3 film with square grid pattern immersed in 1 : 3 $K_2Cr_2O_7$–HCl for 5 seconds. The arrow indicates an over-eroded site on the pattern.

10 nm min^{-1} to a few tens of nanometers per minute as temperature ramps up from 20 °C to 45 °C). While after the $[H^+]$ of the $K_2Cr_2O_7$ etchants is increased larger than 8 mol L^{-1}, the chemical reaction is obviously activated and the etching rates yield rapid increase at elevated temperatures. As judged from the measured rate curves depicted in Fig. 2(b), the dissolution of Bi_2Se_3 in 1 : 3 $K_2Cr_2O_7$–HCl is nearly three times faster than it in 1 : 2 $K_2Cr_2O_7$–HCl etchant at room temperature. To quantitatively describe the chemical reaction intensity of Bi_2Se_3 in the oxidizing acids with different $[H^+]$, we calculate the activation energies of etching reactions of Bi_2Se_3 in 1 : 1, 1 : 2, and 1 : 3 $K_2Cr_2O_7$–HCl solutions (the corresponding $[H^+]$ is 6 mol L^{-1}, 8 mol L^{-1}, and 9 mol L^{-1}, respectively) from the plots using Arrhenius equation for these curves shown in Fig. 2(b), and the calculated activation energies are 0.88 eV, 0.74 eV, and 0.47 eV, respectively. It thus strongly manifests that the chemical reaction barrier of Bi_2Se_3 in the oxidizing acids decreases dramatically as the acidity increases in the etching solutions. However, such an intense reaction leads to severely uneven etching of the patterned film. As shown in inset of Fig. 2(b) is an optical microscopic picture of slightly etched Bi_2Se_3 by 1 : 3 $K_2Cr_2O_7$–HCl solution at room temperature, on which it can be clearly figured out that the areas near the grid corners are attacked much faster than the other regions. As the etching proceeds, undesired "W"-shape depth profiles of the film gradually evolve and part of the Bi_2Se_3 grid pattern gets eventually dissolved.

Almost the same etching behaviors of Bi_2Se_3 in $K_2Cr_2O_7$–H_2SO_4 etchants are observed. The 1 : 2 in $K_2Cr_2O_7$–H_2SO_4 ($[H^+]$: 12 mol L^{-1}) etchant also yields the same etching rate of ~120 nm min^{-1} as obtained in the 1 : 2 in $K_2Cr_2O_7$–HCl and can produce "U" shape etching profiles of the Bi_2Se_3 films. Anyway, the electronic characteristics of electrodes and heterojunctions based on the etched Bi_2Se_3 subject on the microscopic surface properties, it's therefore necessary to analyze the morphologies and stoichiometry of the Bi_2Se_3 surfaces etched by these two kinds of etchants. As illustrated in Fig. 3(a) is a SEM image of an as-deposited Bi_2Se_3 thin film. High dense growth spirals surrounded by straight steps are observed in the as-grown Bi_2Se_3 thin films (highlighted by dashed triangles in Fig. 3(a)). As measured by AFM, the root mean square (RMS) roughness of such surface is ~3 nm (in area of 5 × 5 μm^2), as shown in Table 2. After being immersed in 1 : 2 $K_2Cr_2O_7$–H_2SO_4 solution for 30

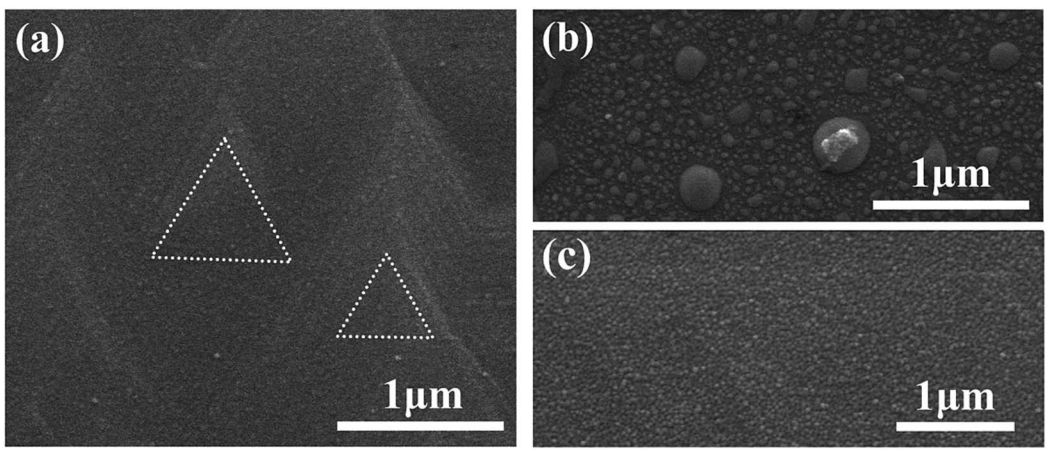

Fig. 3 SEM images of an as-deposited Bi_2Se_3 surface (a) and Bi_2Se_3 surfaces etched in 1 : 2 $K_2Cr_2O_7$–H_2SO_4 etchant (b) and 1 : 2 $K_2Cr_2O_7$–HCl etchant (c), respectively.

Table 2 Bi_2Se_3 thin film RMS roughness and Se : Bi mole ratio before and after etched by 1 : 2 $K_2Cr_2O_7$–HCl (H_2SO_4) etchants

Sample surface	RMS roughness	Se : Bi mole ratio
Un-etched Bi_2Se_3 thin film	3 nm	1.6
In 1 : 2 $K_2Cr_2O_7$–H_2SO_4 solution for 30 s	2.5 nm	1.6
In 1 : 2 $K_2Cr_2O_7$–HCl solution for 30 s	1.5 nm	1.1

seconds which corresponds to an etching depth of ~60 nm, these pyramid morphologies completely vanish and a surface decorated with large amounts of irregular-shaped islands sized from ~20 nm to ~300 nm comes out as exhibited in Fig. 3(b). The surface morphology does not improve too much (RMS roughness ~2.5 nm) as compared to the as-deposited Bi_2Se_3 film. On such etched surface, a Se : Bi mole ratio of ~1.60 is detected by EDX measurement. The Se : Bi mole ratio doesn't change significantly after a further 30 seconds etching period indicates a stoichiometric dissolution of Bi_2Se_3 in the 1 : 2 in $K_2Cr_2O_7$–H_2SO_4 etchant. Fig. 3(c) shows a SEM image taken from a Bi_2Se_3 film etched in 1 : 2 in $K_2Cr_2O_7$–HCl solution at ~60 nm depth too. A much smoother surface (RMS roughness ~1.5 nm) is obtained for Bi_2Se_3 in this etchant. Not identical to the case of Bi_2Se_3 in 1 : 2 in $K_2Cr_2O_7$–H_2SO_4, Se : Bi mole ratio on the 1 : 2 in $K_2Cr_2O_7$–HCl etched surface is ~1.1 as measured by EDX, implying a Se-dissolving preferred reaction kinetics. As etching proceeds to ~270 nm depth, only Bi signal from the film can be detected by EDX indicating a full depletion of Se. It should be noted that the good epitaxial character with two-dimensional surface terrace-step structures of initial Bi_2Se_3 films disappears after being etched in both solutions, which strongly implies that both etching processes would cause amorphous surface parts of the Bi_2Se_3 films. It's thus also reasonable to attribute the nano-sized islands with irregular shapes (as shown in Fig. 3(b) and (c)) to be amorphous Bi_2Se_3 deposits after etching.

It's well known that wet chemical etching proceeds by oxidation of the semiconductor constituents followed by chemical dissolution of the oxides in suitable solvents. For etching covalent chalcogenides such as CdSe, CdTe, and HgCdTe, different dissolving rates between cations and chalcogens are often observed because the hydration of cations is much easier than that of nonfully-oxidized chalcogens on the material surfaces.[26–29] As a result, the etched surfaces of chalcogenides are usually cation-deficient. While no cation-deficient surfaces of etched Bi_2Se_3 are obtained in our experiments, which suggests quite different reaction kinetics of layered Bi_2Se_3 as compared to that of covalent chalcogenides in oxidizing acids etchants. To further understand the chemical reaction kinetics of Bi_2Se_3 in oxidizing acids with different components, XPS study is carried out for characterizing the chemical status of Bi_2Se_3 surfaces etched in different acid $K_2Cr_2O_7$ solutions.

As shown in Fig. 4 are core level spectrum of Bi and Se elements detected by XPS from the samples etched in 1 : 2 $K_2Cr_2O_7$–HCl and 1 : 2 $K_2Cr_2O_7$–H_2SO_4 etchants with etching depth of ~60 nm, respectively. The binding energies (BE) obtained in the XPS analysis are standardized for specimen charging using C 1s peak as the reference at 284.8 eV. To precisely determine the peaks' positions, Lorentz–Gauss profiles and Shirley background have been taken for the deconvolution. As indicated in Fig. 4(a) is Bi 4f spectrum from the $K_2Cr_2O_7$–H_2SO_4 etched Bi_2Se_3 sample, in which the intensity contribution for spin–orbit-splitting Bi 4f peaks ($4f_{7/2}$ and $4f_{5/2}$) from either Bi–O bonding[30,31] or Bi–Se bonding can be clearly distinguished upon deconvolution. The intensities of Bi–O bonding Bi peaks are much stronger than that of Bi–Se bonding Bi peaks, which suggest there exists a bismuth oxide (BiO_x) thin layer deposited on the Bi_2Se_3 surface during etching. While for the $K_2Cr_2O_7$–HCl etched Bi_2Se_3 case, only a pair of Bi 4f peaks located at 158.82 eV and 164.11 eV are observed which can be

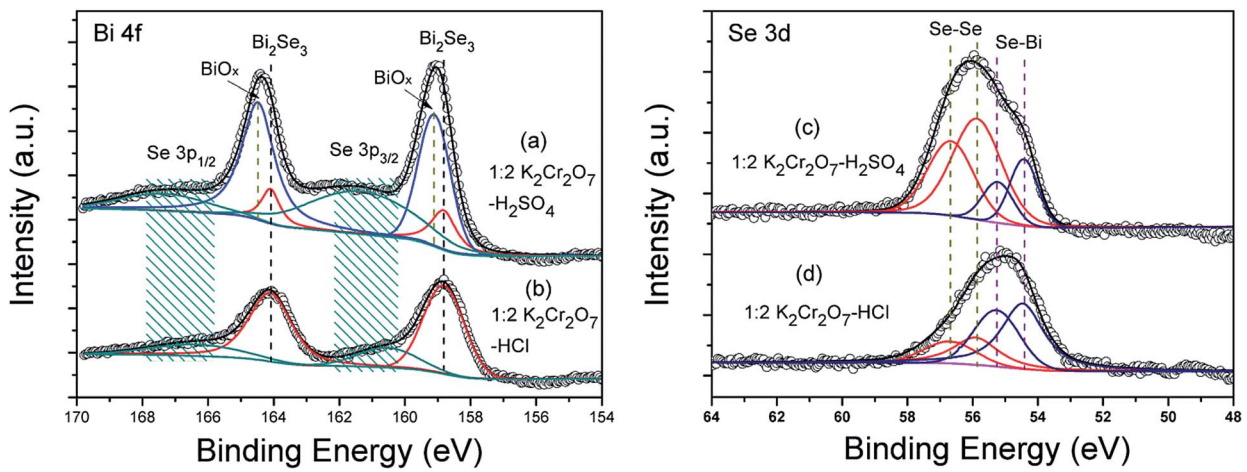

Fig. 4 Bi 4f and Se 3d XPS spectra of Bi_2Se_3 films after etched by 1 : 2 $K_2Cr_2O_7$–H_2SO_4 etchant [(a) and (c)] and by 1 : 2 $K_2Cr_2O_7$–HCl etchant [(b) and (d)], respectively. Experimental data are the open circles and fits are the solid lines.

precisely attributed to Bi–Se bonding of pure Bi_2Se_3 (Fig. 4(b)).[32–34] Peaks referred to Se $3p_{1/2}$ and Se $3p_{3/2}$ can also be figured out in both fitted XPS spectra as exhibited in Fig. 4(a) and (b), and the broaden peak profiles depict a mixed valence states of Se on both samples.[35] The valence states of Se from Bi_2Se_3 films after etched by $K_2Cr_2O_7$–H_2SO_4 and $K_2Cr_2O_7$–HCl are further investigated by analyzing the peak fitted Se 3d ($3d_{5/2}$ and $3d_{3/2}$) spectra as illustrated in Fig. 4(c) and (d), respectively. In either Se 3d curve, the pair of high BE component peaks belong to Se–Se bonding of element Se and the other pair are related to Bi–Se bonding, respectively. And no traces of any selenium oxides can be found on the etched Bi_2Se_3 surfaces in our XPS studies.[30] Therefore, it's reasonable to determine that there's only a $Se^{2-} \rightarrow Se^0$ oxidizing reaction happens for the Se element in both etching processes and the free element Se reactants are deposited onto the Bi_2Se_3 surfaces. Further, peak intensity contribution from Se–Se bonding dominates in Se 3d spectra of the $K_2Cr_2O_7$–H_2SO_4 etched Bi_2Se_3 sample while it becomes not prominent in $K_2Cr_2O_7$–HCl etched one, which manifests that there're more Se deposits residual on $K_2Cr_2O_7$–H_2SO_4 etched Bi_2Se_3 surface than those on $K_2Cr_2O_7$–HCl etched one.

Based on the XPS observations, it should be feasible to determine that the surface chemistry is predominated by bismuth oxides and element Se all through the etching procedure in $K_2Cr_2O_7$–H_2SO_4 solutions. Therefore the surface reaction kinetics are only subjected by the rate of reactants reaches and leaves the etched surface.[36] As to our knowledge, there's only tempered chemical reactions happen between bismuth oxides and concentrated acids (such as H_2SO_4 and HCl) at room temperature. So do them between element Se and concentrated sulphuric acid. As a result, congruently dissolving of Bi and Se will dominate in the etching reaction which is confirmed by our experiment observations.

On the other hand, the valence states of Bi in Bi_2Se_3 remains intact during etching in $K_2Cr_2O_7$–HCl solutions. It's thus suggested that the etching action on the Bi_2Se_3 surface is fully triggered by dissolving of Se. As a result, it leads to the observed incongruently etching behaviors of Bi_2Se_3 in $K_2Cr_2O_7$–HCl etchants.

4. Conclusions

To summary, mesa-shaped etching profile of Bi_2Se_3 is obtained either in 1 : 2 $K_2Cr_2O_7$–HCl or 1 : 2 $K_2Cr_2O_7$–H_2SO_4 aqueous solutions with H^+ concentrations of 8 mol L^{-1} and 12 mol L^{-1}, respectively. Dissolving rates of Bi_2Se_3 are approximately 120 nm min^{-1} in both the 1 : 2 $K_2Cr_2O_7$–H_2SO_4 and 1 : 2 $K_2Cr_2O_7$–HCl etchants at room temperature. Though either etchant is qualified for preparing desired microscopic patterns of Bi_2Se_3, quite distinct dissolving kinetics between these two etchants significantly lead to different reaction products on surfaces of the etched samples. In 1 : 2 $K_2Cr_2O_7$–H_2SO_4 etching case, the surface stoichiometry of Bi_2Se_3 is found intact that the TI surface states would probably being reserved after etching. While the Se-deficient dissolving behavior of Bi_2Se_3 noted in the $K_2Cr_2O_7$–HCl etchants implies surface quality degradation. Nevertheless, slightly metal-rich surface may benefit a low-resistance ohmic contact formation between Bi_2Se_3 and electrode metals that has been argued crucial for improving performance of TE devices.[37] Considering chemical treatment of semiconductor surfaces is a convenient way to define the surface properties and manufacture micropatterns, our findings may serve as useful reference for fabricating Bi_2Se_3-based devices with various purpose.

Acknowledgements

This work is supported by the National Natural Science Foundation of China (Grant No. 11104010, 61474014, 51272038, and 51302030) and Open Research Fund Program of the State Key Laboratory of Low-Dimentional Quantum Physics (No. 20120910).

References

1 C. Wood, *Rep. Prog. Phys.*, 1988, **51**, 459–539.
2 G. Chen, M. S. Dresselhaus, G. Dresselhaus, J. P. Fleurial and T. Caillat, *Int. Mater. Rev.*, 2003, **48**, 45–66.
3 D. Hsieh, Y. Xia, D. Qian, L. Wray, F. Meier, J. H. Dil, J. Osterwalder, L. Patthey, A. V. Fedorov, H. Lin, A. Bansil, D. Grauer, Y. S. Hor, R. J. Cava and M. Z. Hasan, *Phys. Rev. Lett.*, 2009, **103**, 4.
4 Y. Xia, D. Qian, D. Hsieh, L. Wray, A. Pal, H. Lin, A. Bansil, D. Grauer, Y. S. Hor, R. J. Cava and M. Z. Hasan, *Nat. Phys.*, 2009, **5**, 398–402.
5 H. Zhang, C. X. Liu, X. L. Qi, X. Dai, Z. Fang and S. C. Zhang, *Nat. Phys.*, 2009, **5**, 438–442.
6 H. L. Peng, K. J. Lai, D. S. Kong, S. Meister, Y. L. Chen, X. L. Qi, S. C. Zhang, Z. X. Shen and Y. Cui, *Nat. Mater.*, 2010, **9**, 225–229.
7 J. Chen, H. J. Qin, F. Yang, J. Liu, T. Guan, F. M. Qu, G. H. Zhang, J. R. Shi, X. C. Xie, C. L. Yang, K. H. Wu, Y. Q. Li and L. Lu, *Phys. Rev. Lett.*, 2010, **105**, 4.
8 J. Wang, H. Li, C. Chang, K. He, J. S. Lee, H. Lu, Y. Sun, X. Ma, N. Samarth and S. Shen, *Nano Res.*, 2011, **5**, 739–746.
9 G. H. Zhang, H. J. Qin, J. Teng, J. D. Guo, Q. L. Guo, X. Dai, Z. Fang and K. H. Wu, *Appl. Phys. Lett.*, 2009, **95**, 3.
10 H. D. Li, Z. Y. Wang, X. Kan, X. Guo, H. T. He, Z. Wang, J. N. Wang, T. L. Wong, N. Wang and M. H. Xie, *New J. Phys.*, 2010, **12**, 11.
11 H. D. Li, L. Gao, H. Li, G. Y. Wang, J. Wu, Z. H. Zhou and Z. M. Wang, *Appl. Phys. Lett.*, 2013, **102**, 4.
12 A. Richardella, D. M. Zhang, J. S. Lee, A. Koser, D. W. Rench, A. L. Yeats, B. B. Buckley, D. D. Awschalom and N. Samarth, *Appl. Phys. Lett.*, 2010, **97**, 3.
13 X. Guo, Z. J. Xu, H. C. Liu, B. Zhao, X. Q. Dai, H. T. He, J. N. Wang, H. J. Liu, W. K. Ho and M. H. Xie, *Appl. Phys. Lett.*, 2013, **102**, 4.
14 S. Schreyeck, N. V. Tarakina, G. Karczewski, C. Schumacher, T. Borzenko, C. Brune, H. Buhmann, C. Gould, K. Brunner and L. W. Molenkamp, *Appl. Phys. Lett.*, 2013, **102**, 4.
15 S. Augustine and E. Mathai, *Mater. Res. Bull.*, 2001, **36**, 2251–2261.

16 C. Shafai and M. J. Brett, *J. Vac. Sci. Technol., A*, 1997, **15**, 2798–2801.
17 L. M. Goncalves, J. G. Rocha, C. Couto, P. Alpuim, G. Min, D. M. Rowe and J. H. Correia, *J. Micromech. Microeng.*, 2007, **17**, S168–S173.
18 L. M. Goncalves, C. Couto, P. Alpuim and J. H. Correia, *J. Micromech. Microeng.*, 2008, **18**, 1171–1185.
19 J. P. Carmo, L. M. Goncalves and J. H. Correia, *IEEE Trans. Ind. Electron.*, 2010, **57**, 861–867.
20 L. M. Goncalves, P. Alpuim and J. H. Correia, *J. Electron. Mater.*, 2010, **39**, 1516–1521.
21 J. P. Carmo, M. F. Silva, J. F. Ribeiro, R. F. Wolffenbuttel, P. Alpuim, J. G. Rocha, L. M. Goncalves and J. H. Correia, *Microsyst. Technol.*, 2011, **17**, 1283–1291.
22 T. Ngai and U. Ghoshal, Wet etching of Bi2Te3 thin films compatible with microelectronic fabrication processes, *26th International Conference on Thermoelectrics*, Jeju, Korea, June 2007.
23 S. Adachi, H. Kawaguchi and G. Iwane, *J. Mater. Sci.*, 1981, **16**, 2449–2456.
24 J. Zhang, Z. P. Peng, A. Soni, Y. Y. Zhao, Y. Xiong, B. Peng, J. B. Wang, M. S. Dresselhaus and Q. H. Xiong, *Nano Lett.*, 2011, **11**, 2407–2414.
25 K. M. F. Shahil, M. Z. Hossain, V. Goyal and A. A. Balandin, *J. Appl. Phys.*, 2012, **111**, 8.
26 R. Tenne and G. Hodes, *Appl. Phys. Lett.*, 1980, **37**, 428–430.
27 W. H. Chang, T. Lee and W. M. Lau, *J. Appl. Phys.*, 1990, **68**, 4816–4819.
28 I. M. Kotina, L. M. Tukhkonen, G. V. Patsekina, A. V. Shchukarev and G. M. Gusinskii, *Semicond. Sci. Technol.*, 1998, **13**, 890–894.
29 V. Srivastav, R. Pal and H. P. Vyas, *Opto-Electron. Rev.*, 2005, **13**, 197–211.
30 D. Kong, J. J. Cha, K. Lai, H. Peng, J. G. Analytis, S. Meister, Y. Chen, H. J. Zhang, I. R. Fisher and Z. X. Shen, *ACS Nano*, 2011, **5**, 4698–4703.
31 A. J. Green, S. Dey, Y. Q. An, B. O'Brien, S. J. O'Mullane, B. Thiel and A. C. Diebold, 2016, arXiv: cond-mat.mtrl-sci/1601.04057.
32 V. V. Atuchin, V. A. Golyashov, K. A. Kokh, I. V. Korolkov, A. S. Kozhukhov, V. N. Kruchinin, S. V. Makarenko, L. D. Pokrovsky, I. P. Prosvirin, K. N. Romanyuk and O. E. Tereshchenko, *Cryst. Growth Des.*, 2011, **11**, 5507–5514.
33 M. T. Edmonds, J. T. Hellerstedt, A. Tadich, A. Schenk, K. M. O'Donnell, J. Tosado, N. P. Butch, P. Syers, J. Paglione and M. S. Fuhrer, *J. Phys. Chem. C*, 2014, **118**, 20413–20419.
34 C. Han, J. Yang, C. Yan, Y. Li, F. Y. Liu, L. X. Jiang, J. C. Ye and Y. X. Liu, *CrystEngComm*, 2014, **16**, 2823–2834.
35 V. A. Golyashov, K. A. Kokh, S. V. Makarenko, K. N. Romanyuk, I. P. Prosvirin, A. V. Kalinkin, O. E. Tereshchenko, A. S. Kozhukhov, D. V. Sheglov, S. V. Eremeev, S. D. Borisova and E. V. Chulkov, *J. Appl. Phys.*, 2012, **112**, 4.
36 Y. C. Lin, Y. C. Jian and J. H. Jiang, *Appl. Surf. Sci.*, 2008, **254**, 2671–2677.
37 M. Hines, J. Lenhardt, M. Lu, L. Jiang and Z. Xiao, *J. Vac. Sci. Technol., A*, 2012, **30**, 041509.